ISSN 0001-4370, Oceanology, 2014, Vol. 54, No. 6, pp. 688–694. © Pleiades Publishing, Inc., 2014.
Original Russian Text © B.N. Filyushkin, M.A. Sokolovskiy, N.G. Kozhelupova, I.M. Vagina, 2014, published in Okeanologiya, 2014, Vol. 54, No. 6, pp. 737–743.

MARINE PHYSICS

Lagrangian Methods for Observation of Intrathermocline Eddies in Ocean

B. N. Filyushkin[a], M. A. Sokolovskiy[b], N. G. Kozhelupova[a], and I. M. Vagina[c]

[a] *Shirshov Institute of Oceanology, Russian Academy of Sciences, Moscow, Russia*
e-mail: borfil@ioran.ru; nk@ioran.ru
[b] *Water Problems Institute, Russian Academy of Sciences, Moscow, Russia*
e-mail: sokol@aqua.laser.ru
[c] *Moscow State University, Moscow, Russia*
e-mail: iravag@rambler.ru

Received April 8, 2014

Abstract—Intrathermocline anticyclonic eddies (lenses) of Mediterranean origin are regularly observed in the Eastern part of the Atlantic Ocean. These eddies are identified both from satellites as altimetry and sea-surface temperature (SST) changes and according to data of neutral buoyancy floats (NBF) placed in the body of a lens. In this paper, in the framework of a three-layer quasi-geostrophic model, using the contour dynamics method, we consider some theoretical aspects of lens movement observations made by acoustic NBF and freely drifting buoys of the Argo project. Direct experimental observation data on the lenses' drift in the North Atlantic qualitatively confirmed the results of our numerical experiments. In particular, it is shown that the spin of the lens has an advective influence on the behavior of NBF at distances of several lens radii.

DOI: 10.1134/S0001437014050051

Intrathermocline anticyclonic eddies (lenses) are regularly observed at mid-latitudes in the northeastern Atlantic ocean at intermediate depths of 500–1500 m [1, 6, 12]. They are shaped as elliptic structures with horizontal axes from 40 to 100 km and the vertical ones from 0.4 to 0.9 km and filled with warm and salty Mediterranean waters. The difference of the water characteristics in the lens core and the surrounding waters varies from 1 to 4°C in temperature and from 0.3 to 1.0 PSU in salinity depending on the distance of the lens from the region of its formation. The lifetime of such eddies ranges from 3 to 7 years. Roughly 150–200 eddies may simultaneously occur in this part of the ocean [3, 9].

These lenses are usually detected due to hydrological area surveys, in vertical sections, and in course of analysis of the profilograph observational data obtained during the Argo Global Oceanographic Project (the name goes back to the legendary ship of the Argonauts in Greek mythology). During the process of these eddies' interaction with the ambient water, they can transmit their dynamical signal to the surface of the ocean [1, 4, 8]. These vortices are identifiable in altimetric satellite images of the ocean surface level [4, 8], as well as from anomalies of SST [14, 15].

Thus, the satellite observations allow to obtaining the evolution pattern both of the surface eddies and the processes of merging and separation of intrathermocline lenses and their interaction with different features of the bottom relief. Unfortunately, as yet, the correlation of eddy positions obtained from satellite observations and hydrological measurements is insufficiently reliable.

For these reasons, it is expedient to use neutral buoyancy floats (NBF) for long-term observations of the eddy travels in the ocean by deploying the NBFs into the lens bodies. A large-scale experiment was fulfilled in 1984–1986 when the displacements of three lenses were monitored for two years by acoustic NBFs [6, 12]. These lenses measured about 100 km in diameter and roughly 800 m in thickness, and their cores were located at a depth of about 1100 m.

In the present study we examine some theoretical aspects of the lens observations by applying the both methods.

We use the three-layer quasi-geostrophic model [2, 3], where the lenses are understood as the middle layer eddy patches, while the NBFs are related to the centers of passive small initially circular domains of fluid belonging either to the lens or to its vicinity. The model parameters are: the average ocean depth being of $H = 4000$ m, the upper, middle, and lower layers are considered to be $H_1 = 600$ m, $H_2 = 1000$ m, and $H_3 = 2400$ m thick (for the dimensionless layer thicknesses, we have $h_1 = 0.15$, $h_2 = 0.25$, and $h_3 = 0.6$), while the first and the second radii of deformation are $Rd_1 = 32$ km and $Rd_2 = 15$ km. These values are characteristic of the northeastern Atlantic. Under such conditions, the middle layer occupies the depths from 600 to 1600 m. We take Rd_1 as the horizontal length scale.

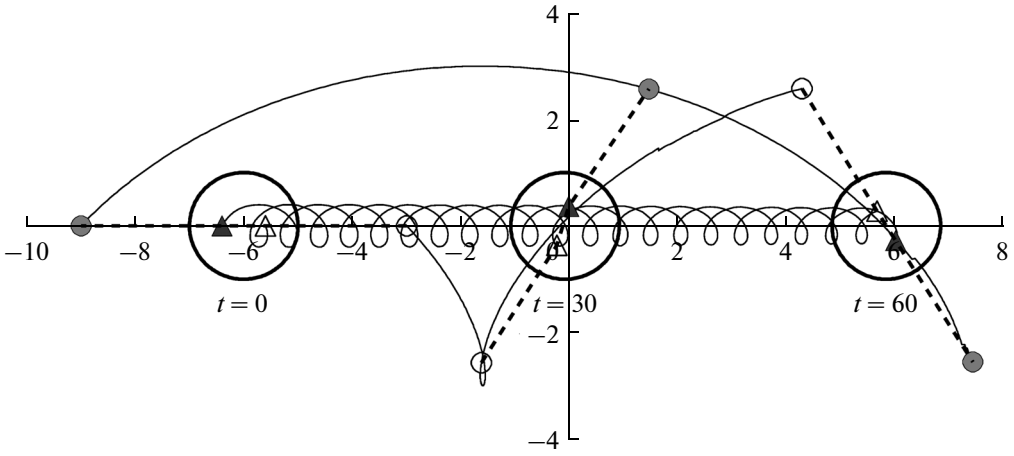

Fig. 1. Configurations of an initially circular lens (bold closed lines) at specified time instants of the dimensionless time t and the trajectories of four model NBFs (thin lines) in the barotropic zonal eastern flow. The external (inner) NBFs are given as filled and empty circular (triangular) markers. The markers are connected with dashed lines to denote their positions at the time instants $t = 0$, 30, and 60.

Figure 1 shows trajectories of four model NBFs that initially occupied the following positions: all of them belong to the same straight line; two of them are placed inside a circular lens at a distance of 0.4 of the lens radius from its center, while another two NBFs are outside the lens at a distance of 3 radii from the center. The dimensionless radius of a circle equals to unity; i.e., the diameter of the simulated lens makes up 64 km, and the dimensionless time unit corresponds to one day. The eddy is transported by an eastward zonal barotropic flow whose velocity makes up 7.41 cm/s at the selected scales. Obviously, in this simplest situation, the lens moves rectilinearly while keeping its shape practically unchanged (the contours of the lens are given in the figure for instants 0, 30, and 60), and internal NBFs rotate around its center with the orbital speed of the fluid particles at the same distance from the center. As a result, these NBFs describe spirals shifted relative to each other by a half-period. A considerable part of the lens M1 trajectories in the experiment of 1984–1986 [6, 11, 12] and the trajectories of NBFs 171, 175, and 177 in the experiment of 1993–1995 in [13] look just in this way. During the whole observation period of the lens M1, the NBFs were located inside the lens and anticyclonically rotated with a period of 6 days. This period remained constant for two years despite the considerable decrease of the lens volume because of mixing at its external boundaries. Note that such constancy of the rotational period of elliptic eddies is corroborated by numerical simulations within the framework of the diffusion model in [10, 16].

The trajectories of external NBFs are more complicated. Being jointly impacted by relatively weak rotational lens forcing and by the main current, they are loop-shaped and periodic. In Fig. 1, the center of the lens initially locates at the point (–6; 0), while the NBFs begin their movements from points (–9; 0) and (–3; 0); the calculation interval makes less than half the period of the revolution of these floats around the lens. Among others, this numerical experiment demonstrates that the lens affects the flow within a distance considerably exceeding its radius.

Figure 2 shows the extent of such motionless circular lens effect (i.e., in the absence of an external current) on a set of surrounding artificially perturbed marker lines. Their unperturbed radii R make up 1.5, 2.0, ..., and 4.5, and the perturbations in the form of the eighth harmonic mode have the amplitude 0.05 (panels (a)) and 0.1 (panels (b)) of the radius length. We see the entrainments that emerged at the time $t = 15$, i.e., in 15 days, in contours with radii R from 1.5 to 2.5 in the first case and up to 3.5 in the second one. The lens influence occurs to be quite perceptible at distances up to $R = 4$.

In the real ocean, it is difficult to monitoring the behavior of NBFs outside the lens itself, but within the zone of its influence. The observations of the lens M1 interaction with two acoustic NBFs are described in [12] (Fig. 7 in [12] involves floats 126 and 132). We reproduce here this figure after minor adaptations (see Fig. 3). The lens M1, 50 km in radius and 0.8 km in thickness, drifts southwards at depths of 700 to 1500 m with velocity of 1.8 cm/s (measured at the 1100 m depth), while the acoustic NBFs move northwestwards at the same depth with velocity of 0.3 cm/s at the distances about 300 and 60 km from the lens M1 center. The remote NBF (126) when reaching the latitude of the lens, describes a loop, coming nearer to the lens by 150 km, and then it runs away westwards by more than 350 km as if it returns for continuation of its initial trajectory. At the same time, NBF 132, initially located at the edge of the lens, describes an intricate trajectory consistent of several loops: it moves north- and west-

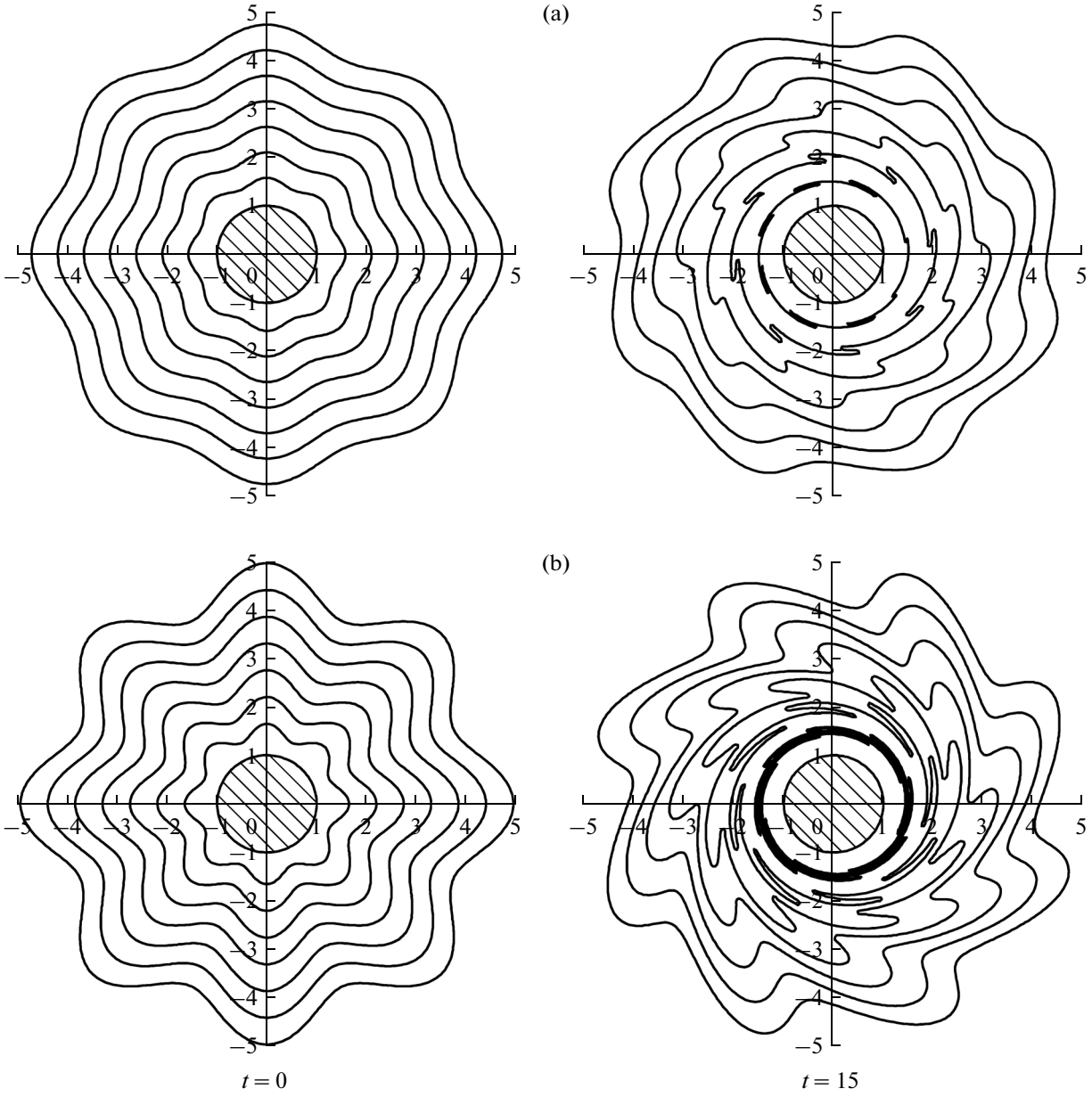

Fig. 2. The forcing of a circular lens of unit radius (shaded area) upon the surrounding seven disturbed marker contours with the mean radii R from 1.5 to 4.5 with a 0.5 step and the amplitude of the disturbance $\Delta = 0.05R$ (a) and $\Delta = 0.1R$ (b).

wards by 150–200 km; next it comes from the north closer to the lens by 100 km; and, finally, returns to the northward drift opposite to the motion of the lens. These observations allow us to note that the lens entrainment effect upon the separate external NBFs is traceable as far as $6R$. The lens-NBF interaction is complicated at distances shorter than $3R$. The estimates from our model calculations (Figs. 1 and 2) provide qualitative corroboration of the above pattern of the NBFs and lens interaction.

Here, it should be noticed a circumstance that impedes the analysis of a lens and a NBF interaction. The lens is a whole rotating body which occupies a volume in the layer of 700–1500 m and moves at an integral velocity within this layer. At the same time, the NBFs are usually placed in the center of the lens core. As soon as NBFs leave the lens, they drift with a velocity, characteristic for the depth of 1100 m. In this case, the pattern of the vertical variations of the hydrophysical features outside the lens can substantially differ, what may explain the fact of the deviation of the NBFs and lens drift directions in Fig. 3.

The numerical experiment whose results are given in Fig. 4 was aimed at the following: (*1*) to compare the

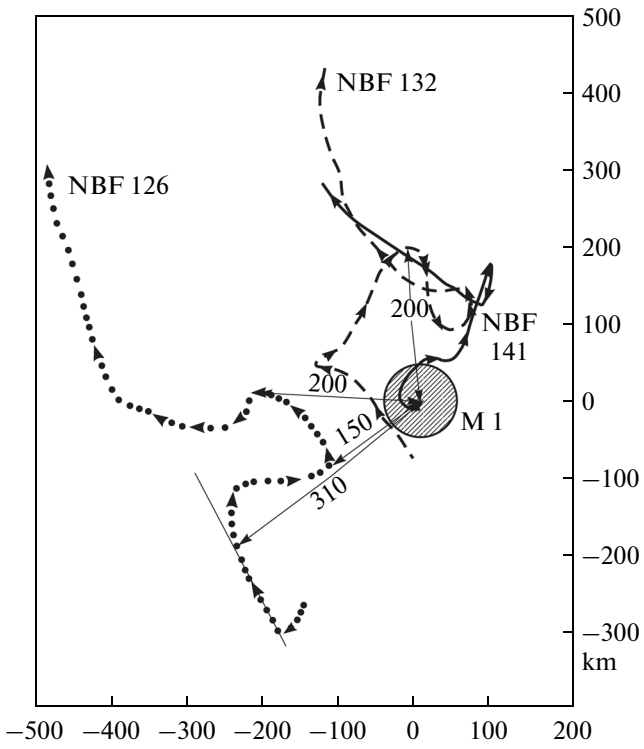

Fig. 3. Trajectories of three NBFs (126, 132, and 141) passing in the vicinity of the lens M1 drifting southwards. NBF 141 was placed inside the lens and rotated in the latter along a circular orbit for eight months before leaving the lens. The arrows with digits show the distance to the center of the lens in kilometers (ajusted Fig. 7 from [12]).

Lagrangian characteristics of the NBF (circular marker) and the "Argo" (triangular markers); (*2*) to show that a single marker may be insufficient to follow up intricate lens movements. For numerical calculations, we set model profilographs and represent them in the same manner as the NBFs, but in contrast to the NBFs, they periodically surface into the upper layer every 9 days of the model time, and for one day they move with the flow; further they return to the middle layer. Thus, in each of the panels of this figure, starting from $t = 10$, the triangle marker occupies the place where it comes at the end of its daily stay in the upper layer. The markers of both types were artificially placed in each panel of the figure; at the initial instant they are located in the same point. Here, we have represented the initial lens as an elliptic eddy patch with a semiaxis ratio along the y- and x-directions equal to 1/8, and we placed the markers closer to one of the lens edges. In course of evolution, such elongated lens splits into two parts because of its instability [3, 4, 9]. It is evident from the figure that the Argo buoy gradually lags behind the NBF after each surfacing and submersion, and the total lag accumulated during the calculation time turned out to be longer than the full NBF rotation cycle inside the eddy patch. Nevertheless, in this case, it is possible to conclude that both types of markers successfully trace the movement of one part of the lens. On the other hand, this experiment shows that the second part of the disintegrated elliptic lens remained beyond the limits of Lagrangian observations. Such type of return movements of Argo buoys relative to the mean movement direction of a circular lens has been noticed at the salinity section within the layer of 0–2000 m in the data of Argo profiling from January 17 to September 4, 2005 [1]. For instance, Fig. 6b in [1] shows that a lens drifts along the Moroccan coast, but the profiling of March 28 occurred to be located 30 km to the south of that on April 7. Thus, it is evident that the monitoring of the intricate motion of lenses subjected to partial disintegration requires deployment of several markers into the lenses.

The next series of calculations (Fig. 5) partially fills this deficiency. We placed two floats into an initially circular lens. After its disintegration into two parts because of the impact of an underwater obstacle, each of the parts contained a marker that monitored the motion of the respective eddy patch. Only the eddy filament formed in the middle area between the compact parts of the lens was without observations. The filament made up only 8% of the initial volume of the eddy patch. It is of minor dynamical significance and disappears rather rapidly. The height of the cylindrically shaped underwater elevation measures 800 m, and its radius equals the radius of the lens. In every panel of the figure, the presence of the elevation in the lower layer is indicated by a dark round patch. Its

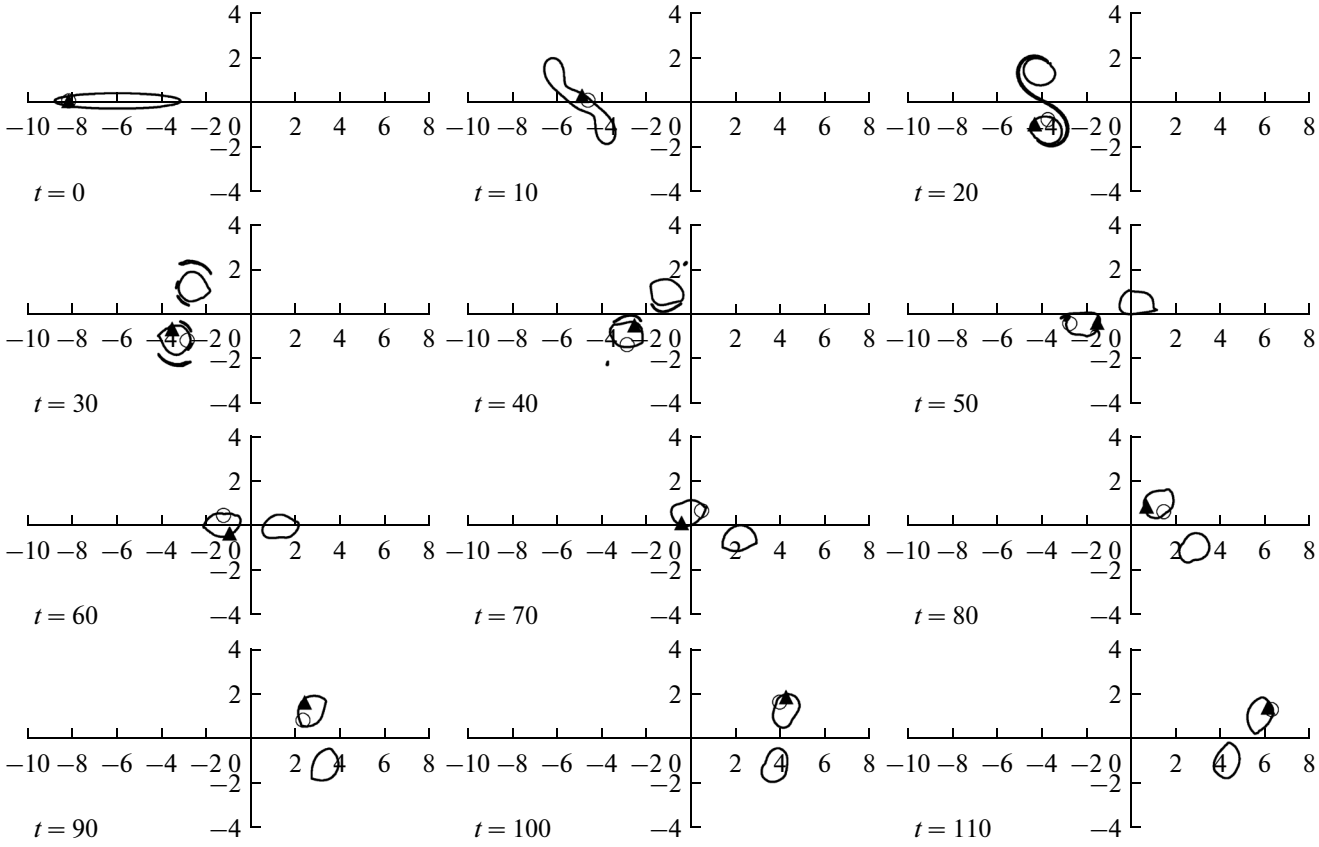

Fig. 4. Instantaneous configurations of an initially elliptic lens (bold closed contours) at specified instants of dimensionless time and locations of model NBFs (light circles) and Argo buoys (dark triangle) in a barotropic zonal eastern flow.

external boundary in the middle and upper layers is designated with a dashed line; thin lines depict imaginary reflections of the lens contours in the upper and lower layers. Additionally, the NBFs, whose horizontal coordinates initially coincided with the positions of the floats in the lens, were deployed in the surface and bottom layers. The main results the experiment are the following:

(1) The behavior of the floats in the upper layer demonstrates that, at least at the beginning of the motion, they reflect the specific features of the movements of the lenses quite adequately (this indirectly corroborates the considerations in [4, 9] concerning the reflection of lenses on the ocean surface), but the relation of the float trajectories and lenses weakens in time.

(2) The floats in the lower layer worsly correspond to the motions of a lens because they are strongly subjected to capturing by the bottom topography.

(3) Two or more (what is desirable) NBFs or Argo buoys placed in a lens are able to serve as fairly reliable Lagrangian markers for studying the lense motions even in cases of their partial disintegration. In part, this simulation result is corroborated by the bihavior of the trajectory of the lens M2 in course of its collision with an underwater mountain [5, 6, 12] and by the movement direction of the NBFs (AMUSE experiment [11]) when they were passing over the Horseshoe seamounts. Joint analysis of the NBFs observations in [11] and the numerical simulation results, has shown [14] that a higher number of NBFs should be placed in separate eddies in order to describe the pattern of the lens disintegration under conditions of irregular bottom topography.

In the ocean, the meeting of an Argo buoy and a lens is a stochastic event. Only 20% of the Argo buoys deployed in the North Atlantic discovered lenses [1]. If a buoy is captured by a lens, it determines the position of the latter and the variations of the temperature and salinity with depth but only at that part of the lense which was the site of profiling. These observations are unable to provide full information of the lens geometry and thermohaline features. Therefore, it is important to use simulation techniques in order to evaluate the informativeness of such observations when studying the intrathermocline eddy dynamics.

In addition, the numerical simulation allowed us to determine more clearly the expected results of the in-

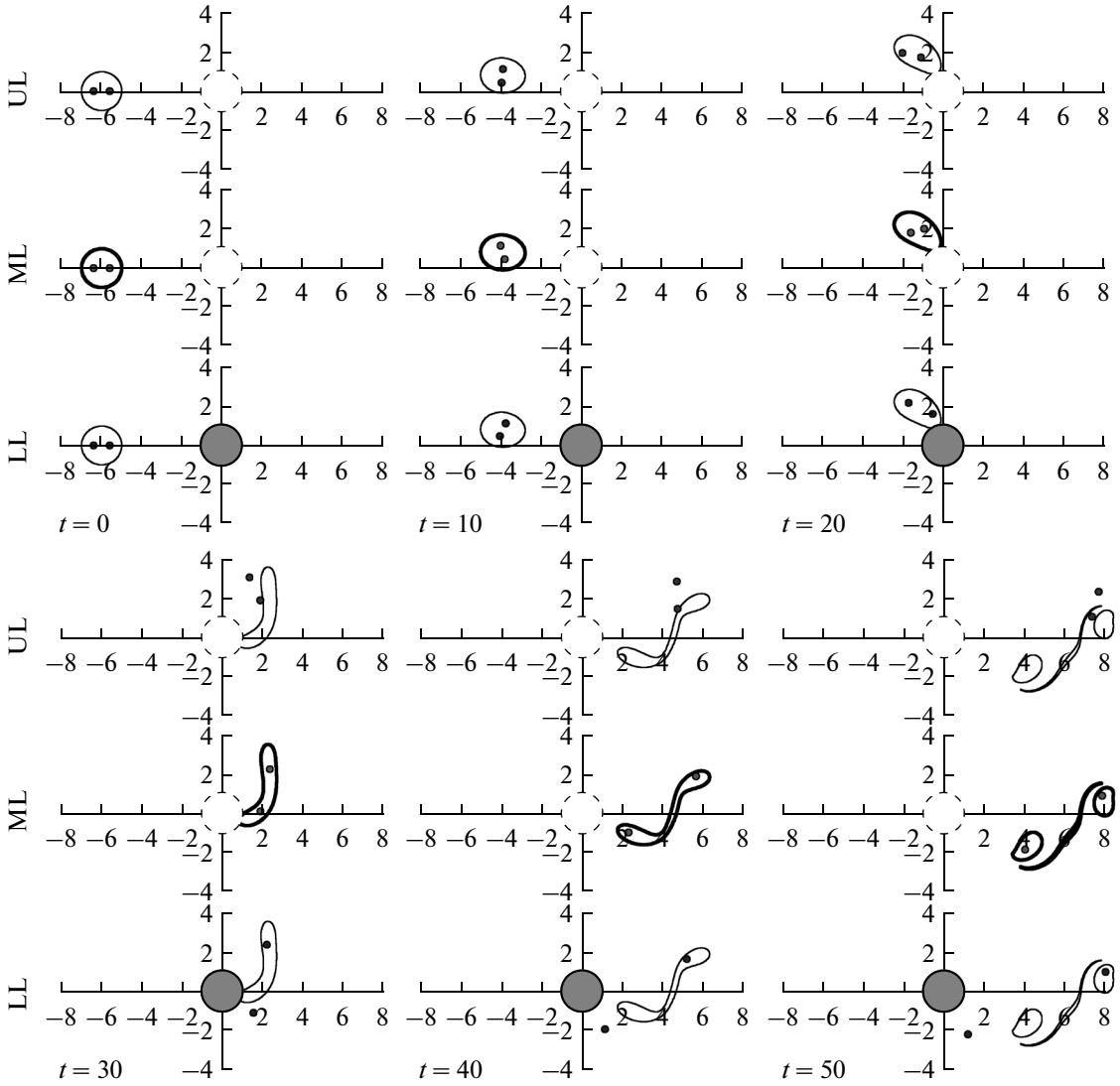

Fig. 5. Instantaneous configurations of an initially circular lens (bold closed contours) and its "reflections" (thin contours) in the upper and lower layers, as well as the positions of two NBFs (dark circles) in each of the layers in a zonal flow running against a circular underwater obstacle located in the lower layer (see the text for details). In every panel, the horizontal synchronous sections of the upper (UL), middle (ML), and lower (LL) layers are given from the top down, respectively.

situ studies concerning the dynamics of the intrathermocline eddies in specific ocean regions. The preliminary calculation results facilitate the development of the requirements for observations by means of satellite altimetry and instrumental observations of current velocities both in the lens itself and beyond the zone affected by the lens using NBFs, Argo buoys, and ADCP current velocimeters [7].

ACKNOWLEDGMENTS

This work was supported by the Russian Foundation for Basic Research, project nos. 13-01-12404, 13-05-00463, and 14-05-00070.

REFERENCES

1. A. N. Demidov, B. N. Filyushkin, and N. G. Kozhelupova, "Detection of Mediterranean lenses in the Atlantic Ocean by profilers of the Argo project," Oceanology (Engl. Transl.) **52** (2), 171–180 (2012).
2. M. A. Sokolovskiy, "Modeling of three-layer vortex movements in the ocean by contour dynamics method," Izv. Akad. Nauk SSSR, Fiz. Atmos. Okeana **27** (5), 550–562 (1991).
3. B. N. Filyushkin, M. A. Sokolovskiy, N. G. Kozhelupova, and I. M. Vagina, "Dynamics of intrathermocline lenses," Dokl. Earth Sci. **434** (2), 1377–1380 (2010).
4. B. N. Filyushkin, M. A. Sokolovskiy, N. G. Kozhelupova, and I. M. Vagina, "Reflection of intrather-

mocline eddies on the ocean surface," Dokl. Earth Sci. **439** (1), 986–989 (2011).

5. B. N. Filyushkin, M. A. Sokolovskiy, N. G. Kozhelupova, and I. M. Vagina, "Evolution of intrathermocline eddies moving over a submarine hill," Dokl. Earth Sci. **441** (2), 1757–1760 (2011).
6. L. Armi, D. Hebert, N. Oakey, et al., "Two years in the life of a Mediterranean salt lens," J. Phys. Oceanogr. **19** (3), 354–370 (1989).
7. I. Bashmachnikov and X. Carton, "Surface signature of Mediterranean water eddies in the Northeastern Atlantic: effect of the upper ocean stratification," Ocean Sci. **8**, 931–943 (2012).
8. X. Carton, N. Daniault, J. Alves, et al., "Meddy dynamics and interaction with neighboring eddies southwest of Portugal: observations and modeling," J. Geophys. Res., C: Oceans Atmos. **115**, 06017 (2010). doi: 10.1029/2009JC005646.
9. B. N. Filyushkin and M. A. Sokolovskiy, "Modeling the evolution of intrathermocline lenses in the Atlantic Ocean," J. Mar. Res. **69** (2–3), 191–220 (2011).
10. K. V. Koshel, E. A. Ryzhov, and V. V. Zhmur, "Diffusion-affected passive scalar transport in an ellipsoidal vortex in a shear flow," Nonlin. Processes Geophys. **20** (4), 437–444 (2013).
11. P. L. Richardson, A. S. Bower, and W. Zenk, "Summary of meddies tracked by floats," Int. WOCE Newslett. **34**, 18–20 (1999).
12. P. L. Richardson, D. Walsh, L. Armi, et al., "Tracking three meddies with SOFAR floats," J. Phys. Oceanogr. **19** (3), 371–383 (1989).
13. P. L. Richardson and C.M. Wooding, "RAFOS float trajectories in meddies during the Semaphore Experiment, 1993–1995," in *Woods Hole Oceanographic Institute, WHOI-99-05, Technical Report*, 1999.
14. M. A. Sokolovskiy, B. N. Filyushkin, and X. J. Carton, "Dynamics of intrathermocline vortices in a gyre flow over a seamount chain," Ocean Dyn. **63** (7), 741–760 (2013).
15. D. Stammer, H.-H. Hinrichsen, and R. H. Käse, "Can meddies be detected by satellite altimetry?" J. Geophys. Res., C: Oceans Atmos. **96** (4), 7005–7014 (1991).
16. V. V. Zhmur, E. A. Ryzhov, and K. V. Koshel, "Ellipsoidal vortex in a nonuniform flow. Dynamics and chaotic advections," J. Mar. Res. **69** (2–3), 435–461 (2011).

Translated by G.S. Karabashev